

# $\Lambda$ production in p+p collisions at 40 and 158 GeV/c

**Herbert Ströbele for the NA61 collaboration**

Universität Frankfurt

E-mail: `stroebel@ikf.uni-frankfurt.de`

**Abstract.** The research programme of the NA61 collaboration covers a wide range of hadronic physics in the CERN SPS energy range. It encompasses measurements of hadron-hadron, hadron-nucleus as well as nucleus-nucleus collisions. The latter are analyzed to better understand the properties of hot and dense nuclear matter. In this contribution we present results on  $\Lambda$  production in proton-proton interactions at beam energies of 40 and 158 GeV/c.

## 1. Introduction

NA61 is a fixed target experiment at the CERN SPS pursuing an ambitious programme in hadron physics using proton and heavy ion beams, as well as in neutrino and cosmic ray physics by measuring hadron-nucleus cross sections as reference data for neutrino flux and atmospheric shower calculations. The subject of the hadron physics programme is the study of the energy region, where the onset of deconfinement is expected to occur. The STAR experiment at RHIC with its Beam Energy Scan programme is also studying this energy range. Next generation experiments at FAIR (CBM) in Darmstadt and NICA in Dubna are planned to follow up with dedicated accelerator facilities. Presently NA61 is the only experiment which does a two-dimensional scan (in energy and system size) of p+p and nuclear collisions. The NA61 detector has an acceptance for charged particles down to  $p_T = 0$  for rapidities forward of mid-rapidity at all energies (20A GeV - 150A GeV). This and its particle identification capabilities allow to determine particle multiplicities in full phase space with small uncertainties introduced by extrapolations into unmeasured regions. In this contribution we present results on  $\Lambda$  production in p+p interactions at beam momenta of 158 and 40 GeV/c.

## 2. The experiment

The main components of the experimental setup are four large volume Time Projection Chambers (TPC) for charged particle tracking and identification by recording the energy loss in the TPC gas. A new small TPC (GTPC) on the beam line records fast forward going particles in p+p interactions [1]. Two time-of-flight walls each covering approximately two square meters improve the kaon identification capabilities. A small scintillator on the beam line downstream of the target is used to veto through-going beams and is used as minimum bias trigger. A hadron calorimeter serves as a projectile spectator detector and is used to select centrality in nuclear collisions.

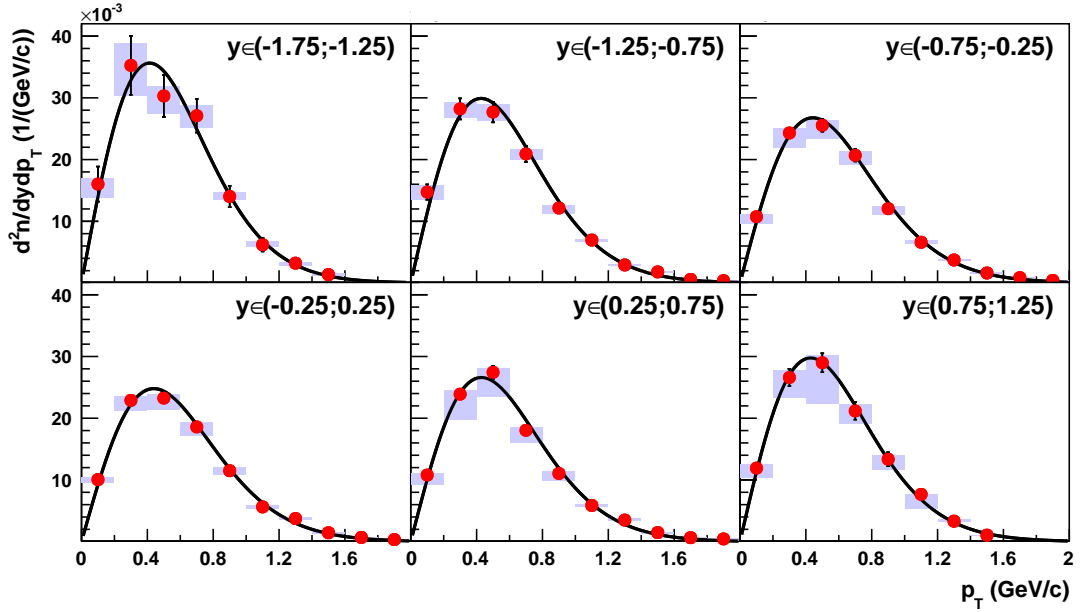


**Figure 1.** Transverse momentum distributions of  $\Lambda$  hyperons in p+p interactions at 158 GeV/c beam momentum. The rapidity intervals in which the  $dn/dp_T$  distributions are obtained are indicated in the individual figures. The lines are the result of fits of Eq.1 to the experimental points. The systematic uncertainties of the  $\Lambda$  yields are indicated by the vertical grey bands at the measured points.

### 3. Results

#### 3.1. $\Lambda$ production in p+p interactions at SPS energies

Candidates of charged decays of  $\Lambda$  hyperons are identified by the standard topological cuts applied to pairs of positively and negatively charged particles. The invariant masses of the resulting candidate decay particles give a distribution which consist of the  $\Lambda$  signal and a

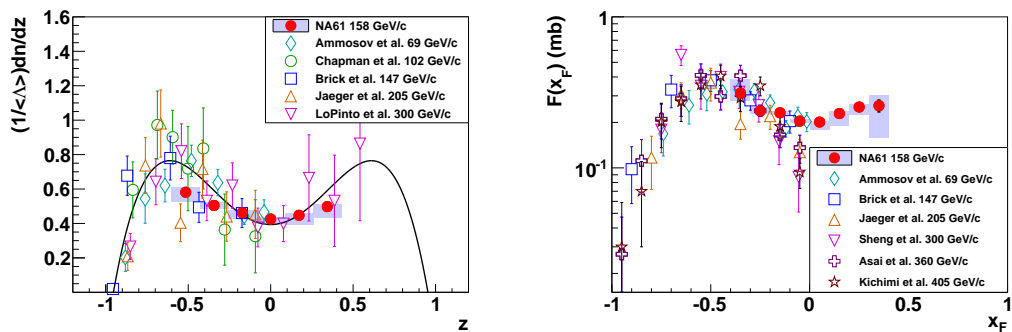


**Figure 2.** (left) Normalized rapidity ( $z=y/y_{beam}$ ) distribution of  $\Lambda$  hyperons produced in p+p interactions at 158 GeV/c together with data from other experiments [3, 4, 5, 6, 7]. A symmetric 4th order polynomial (solid line) is used to estimate the systematic uncertainty of the mean  $\Lambda$  multiplicity (see [2]); (right) same for the invariant cross section as function of  $x_F$ .

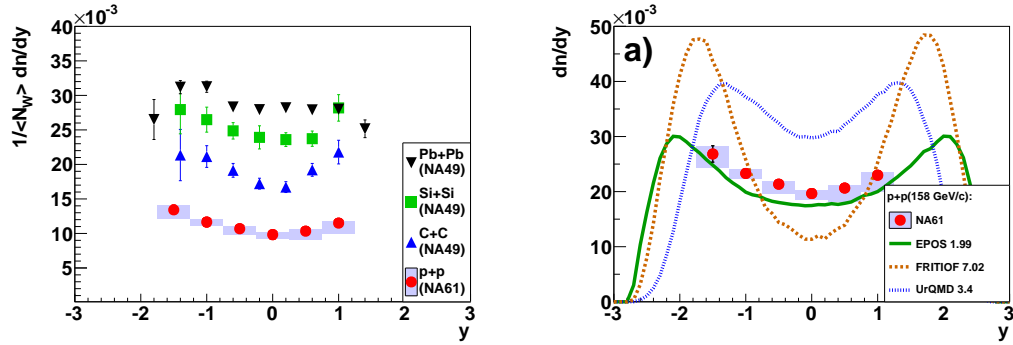


**Figure 3.** (left) Rapidity distribution of  $\Lambda$  hyperons divided by the number of wounded nucleons in inelastic p+p interactions at 158 GeV/c together with the data from Si+Si, C+C [8], and Pb+Pb [9] collisions; (right) comparison of the  $\Lambda$  rapidity distribution in p+p collisions to calculations by the EPOS [10], UrQMD [11, 12], and Fritiof [13] models.

structure-less background. The candidate decay particle pairs populate a large part of the two-dimensional longitudinal rapidity ( $y$ ) or Feynman  $x$  ( $x_F$ ) and transverse momentum ( $p_T$ ) space. A grid in longitudinal and transverse momentum defines phase space cells in which the  $\Lambda$  yields are obtained from fits of signal and background functions to the corresponding invariant mass distributions. These yields are corrected for acceptance and for losses due to the topological and track selection cuts. The yields in phase space cells within a given longitudinal momentum interval form the transverse momentum distributions ( $dn/dp_T$ ). Integration and extrapolation of the transverse momentum distributions provide the data points for  $dn/dy$  and  $dn/dx_F$  distributions. The transverse momentum distributions of  $\Lambda$  shown in Fig.1 are from inelastic p+p collisions at a beam momentum of 158 GeV/c [2]. They cover rapidities from

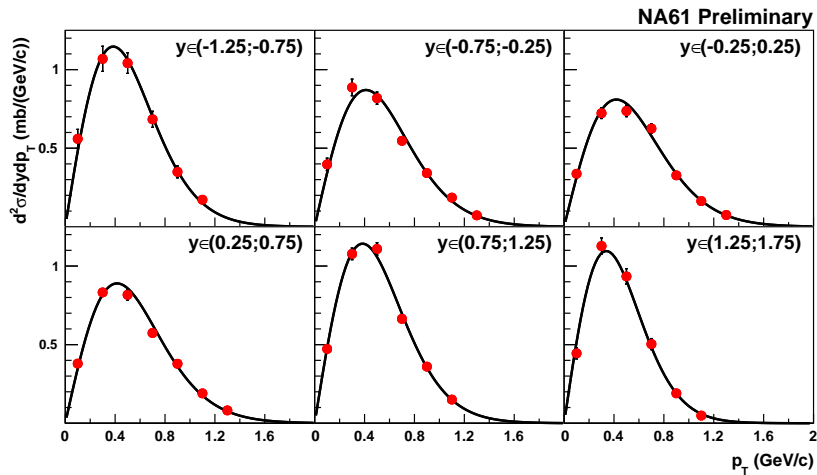


**Figure 4.** Transverse momentum distributions of  $\Lambda$  hyperons in p+p interactions at 40 GeV/c beam momentum. The rapidities at which the  $dn/dp_T$  distributions are obtained are indicated in the individual figures. The lines are the result of fits of Eq.2 to the experimental points.

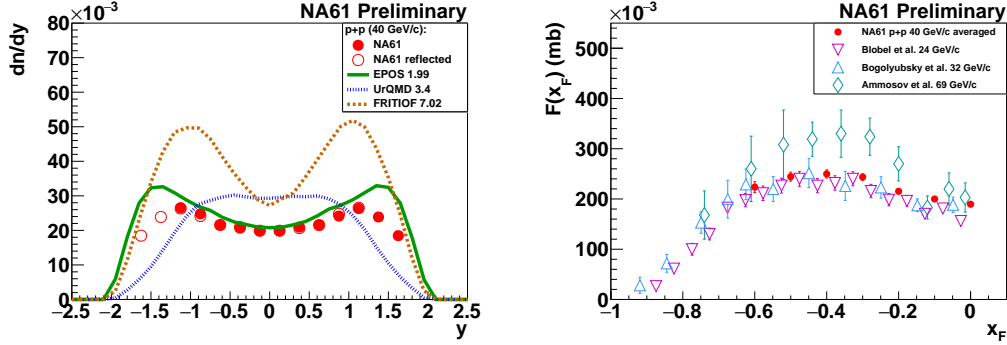


**Figure 5.** (left) Rapidity distribution of  $\Lambda$  hyperons produced in inelastic p+p interactions at 40 GeV/c together with calculations by the EPOS [10], UrQMD [11, 12], and Fritiof [13] models; (right) invariant cross section as function of  $x_F$  of  $\Lambda$  hyperons together with data from other experiments at similar energies [3, 14, 15].

-1.75 to 1.25. The solid lines represent fits of the function

$$\frac{1}{p_T} \frac{d^2n}{dydp_T} = \frac{1}{m_T} \frac{d^2n}{dydm_T} = e^{-m_T/\Gamma}, m_T = \sqrt{p_T^2 + m_\Lambda^2} \quad (1)$$

to the data points which describe the data well. Integration of the  $dn/dydp_T$  distributions in the 6 rapidity intervals provide the 6 data points for the rapidity distribution in Fig.2(left). Also shown are results from other experiments. The mean  $\Lambda$  multiplicity was obtained by extrapolating the  $dn/dx_F$  distribution into the unmeasured region (see [2]). In order to compare with the other measurements at similar energies reduced rapidity ( $z=y/y_{beam}$ ) is used for the abscissa. The NA61 data have statistical uncertainties smaller than the symbol size. The size of the systematic uncertainty is indicated by the grey areas. The world data bracket the high precision NA61 results quite well. The same conclusion can be drawn from Fig.2 (right) in which the invariant  $\Lambda$  cross section is plotted as function of the Feynman x variable ( $x_F$ ) together again with the world data. The measurement by the NA61 collaboration has reduced significantly the uncertainty in the experimental knowledge about  $\Lambda$  production in p+p interactions at SPS energies. Another aspect of measurements of particle production in p+p interactions is their role as reference for studies of nuclear collisions. In Fig.3 (left) we therefore compare the NA61 data on  $\Lambda$  production with the results from Pb+Pb, Si+Si and C+C collisions at the same c.m. energy per nucleon pair. The strangeness enhancement, well established in nuclear collisions, increases with system size in a large range of  $\Lambda$  rapidities. Finally, a comparison with the transport models EPOS and UrQMD as well as with the two-fireball excitation model FRITIOF (Fig.3 right) reveals that only EPOS reproduces the yield and the shape of  $dn/dy$  of the NA61 results on  $\Lambda$  production in p+p interactions.

New preliminary NA61 data on  $\Lambda$  production in p+p interactions at 40 GeV/c beam momentum are presented in the following paragraph. The analysis steps are essentially the same as for the 158 GeV/c data. The resulting  $dn/dp_T$  distributions are shown in Fig.4 together with fits of the function

$$u = A \cdot p_T \cdot e^{-m_T/\Gamma} \quad (2)$$

with  $A$  and  $\Gamma$  as free parameters. The rapidity distribution is again obtained by integration of the  $p_T$  distributions (Fig.5). The statistical uncertainties are smaller than the symbol size. Systematic uncertainties are under study. Since the distribution must be symmetric, the data points can be mirrored at  $y=0$  (open symbols). At 40 GeV/c the covered portion of the rapidity

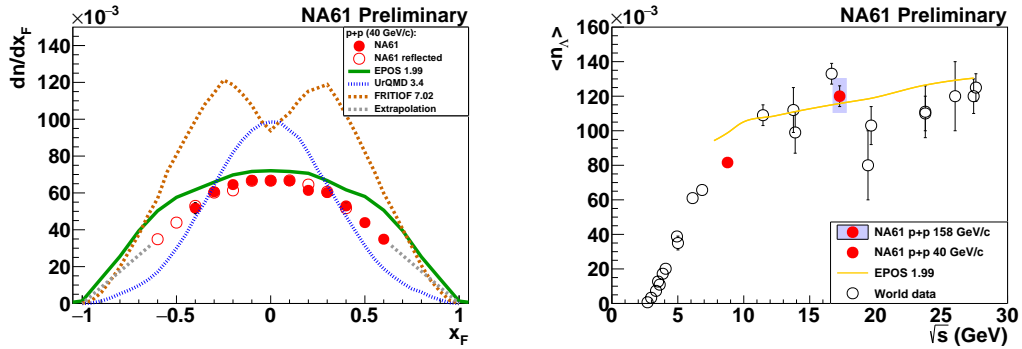


**Figure 6.** (left)  $\Lambda$  hyperon yields in p+p interactions at 40 GeV/c as function of  $x_F$  together with the same model calculations as shown Fig.5. In this form the longitudinal distribution can be extrapolated into the unmeasured region without significant uncertainty (see dotted line); (right)  $\Lambda$  multiplicity in p+p interactions as function of  $\sqrt{s}$  together with world data and results from EPOS [10] calculations.

range is larger than at 158 GeV/c allowing to measure the falling of the leading baryon yield at large rapidities. The comparison to world data is again done using  $z = y/y_{beam}$  as longitudinal variable (Fig.5 right). The same observations can be made as at 158 GeV/c. The preliminary NA61 data have small (statistical) uncertainties and are bracketed well by the world data.

Extrapolation of the  $dn/dx_F$  distribution into the unmeasured regions (see e.g. dotted lines in Fig.6) provides estimates of the  $\Lambda$  yields. The corresponding multiplicities (average yields per event) are compared to world data in Fig.6 (right) as function of c.m. energy ( $\sqrt{s}$ ). The NA61 data follow the trend set by the world data and at the same time reduce uncertainties in the spectral yields significantly at the two energies. Above  $\sqrt{s}=19$  GeV the experimental data have large uncertainties and lie consistently below the EPOS calculation. It is desirable to have new experimental data in this energy range. Below 10 GeV EPOS underestimates  $\Lambda$  yields. However this model is not intended to produce reliable results at this energy and below.

## References

- [1] Abgrall N et al. 2014 *J. Instrum.* **9** P06005
- [2] Aduszkiewicz A et al. 2016 *Eur. Phys. J. C* **76** 198
- [3] Ammosov V et al. 1976 *Nucl. Phys. B* **115** 269
- [4] Chapman J et al. 1973 *Phys.Lett.* **47B** 465
- [5] Brick D et al. 1980 *Nucl. Phys. B* **164** 1
- [6] Jaeger K et al. 1975 *Phys. Rev. D* **11** 2405
- [7] LoPinto F et al. 1980 *Phys. Rev. D* **22** 573
- [8] Alt C et al. 2005 *Phys. Rev. Lett.* **94** 052301
- [9] Alt C et al. 2008 *Phys. Rev. C* **78** 034918
- [10] Werner K, Liu F-M and Pierog T 2006 *Phys. Rev. C* **74** 044902
- [11] Bass S A et al. 1998 *Prog. Part. Nucl. Phys.* **41** 225
- [12] Bleicher M et al. 1999 *J. Phys. G* **25** 1859
- [13] Anderson B, Gustafson G and Hong Pi 1993 *Z. Phys. C* **57** 485
- [14] Blobel V et al. 1974 *Nucl. Phys. B* **69** 454, Blobel V et al. 1978 *Nucl. Phys. B* **135** 379
- [15] Bogolyubsky M et al. 1989 *Sov. J. Nucl. Phys.* **50** 424, *Yad. Fiz.* **50** 683